ARTICLES
https://doi.org/10.1038/s41565-020-0734-1
nature nanotechnology

Enhanced catalytic activity under non-equilibrium conditions

Rui Chen, Simona Neri and Leonard J. Prins ✉

The development of non-equilibrium synthetic systems provides access to innovative materials with life-like properties. Non-equilibrium systems require a continuous input of energy to retain their functional state, which makes for a fundamental difference to systems that operate at thermodynamic equilibrium. Kinetic asymmetry in the energy consumption pathway is required to drive systems out of equilibrium. This understanding has permitted chemists to design dissipative synthetic molecular machines and high-energy materials. Here we show that kinetic asymmetry also emerges at the macroscopic level by demonstrating that local energy delivery in the form of light to a hydrogel containing gold nanoparticles installs a non-equilibrium steady state. The instalment and maintenance of the macroscopic non-equilibrium state is facilitated by the gel matrix in which motion is governed by diffusion rather than convection. The non-equilibrium state is characterized by a persistent gradient in the surface composition of the nanoparticles embedded in the gel, which affects the fluorescent and catalytic properties of the system. We show that the overall catalytic performance of the system is enhanced under these non-equilibrium conditions. In perspective it will be possible to develop out-of-equilibrium matrices in which functional properties emerge as a result of spatially controlled energy delivery and spatially controlled chemistries.

Nature exploits energy to drive chemical processes energetically uphill. The non-equilibrium nature of biological systems manifests itself both at the molecular and macroscopic level[1,2]. The directional motion of motor enzymes[3] and the self-assembly of high-energy structures, such as microtubules[4], exemplify how chemical fuels can drive molecular processes. At the macroscopic level, energy is used to control the chemical composition inside cellular compartments[5] and to install spatial concentration gradients in the cytosol, which are important for many developmental processes[6]. The extraordinary functional properties of the cell are a strong impetus to develop non-equilibrium synthetic systems for innovative applications in materials science and nanotechnology[7–10]. Recent studies have shown how kinetic asymmetry in the energy consumption pathway can drive synthetic molecular machinery[11,12]. Here, we show that kinetic asymmetry can also emerge at the macroscopic scale by demonstrating that local light irradiation of a complex matrix results in a non-equilibrium steady-state distribution of molecules within it. The system relies on the coupling between light-induced conformational change of a photosensitive regulatory element and chemical exchange process that takes place on the surface of nanoparticles. Stable concentration gradients of the regulatory element in the system are maintained as long as energy is locally provided. This concentration gradient is transposed on the surface composition of the nanoparticles and affects the fluorescence and catalytic properties of the system. We also show that diffusion processes installed by light-induced concentration gradients lead to an enhanced catalytic activity in the system under non-equilibrium conditions.

Catalytic nanoparticles with enzyme-like properties

In recent years, we have extensively studied AuNP **1**, which are gold nanoparticles ($d_{Au} \approx 1.8 \pm 0.4$ nm) passivated with alkyl thiols containing a 1,4,7-triazacyclononane (TACN)·Zn^{2+} complex as head group (Fig. 1)[13]. Our interest in these nanoparticles stems from their remarkable catalytic efficiency in the transphosphorylation of 2-hydroxypropyl-4-nitrophenylphosphate (HPNPP), a model substrate for RNA-hydrolysis[14]. A second attractive feature of AuNP **1** is their multivalent cationic monolayer surface that allows small oligoanionic (bio)molecules to bind under saturation conditions at low micromolar concentrations in aqueous buffer[15]. Where different anionic molecules compete for binding to AuNP **1**, the surface coverage is determined by their relative affinities for the monolayer. Where at least one of the molecules is fluorescent, the exchange process can be monitored with fluorescence measurements owing to the quenching of surface-bound fluorophores by the gold core (Fig. 1a)[16]. Recently, we have shown that both the catalytic activity of AuNP **1** and fluorescent probe displacement can be controlled by light using a carboxylic acid-functionalized azobenzene as photosensitive regulatory element[17]. The regulatory effect originated from the different affinities of the *cis*- and *trans*-isomers of azobenzene for AuNP **1** (Fig. 1a). Altogether, AuNP **1** and analogues share many similarities with enzymes—Michaelis–Menten saturation kinetics, cooperative catalysis and competitive binding of inhibitors—and for that reason have been referred to as nanozymes[14,18]. Yet, so far all studies have been performed in diluted solutions, which are poorly comparable with the biological matrices in which natural enzymes are operative. To make for a closer analogy with a natural situation, we were interested in how the chemical processes occurring at the surface of AuNP **1** would be affected by a matrix in which mass transport is controlled by diffusion rather than convection. To that end, we decided to study light-controlled probe displacement and catalytic activity in agarose gel.

Local signal generation through spatially controlled ultraviolet (UV) irradiation

We first improved our light-responsive system to overcome some of the limitations of the previously reported one (Fig. 1a and Supplementary Information)[17]. A new azobenzene derivative **A** was synthesized containing a phosphate group, because previous

Department of Chemical Sciences, University of Padova, Padova, Italy. ✉e-mail: leonard.prins@unipd.it

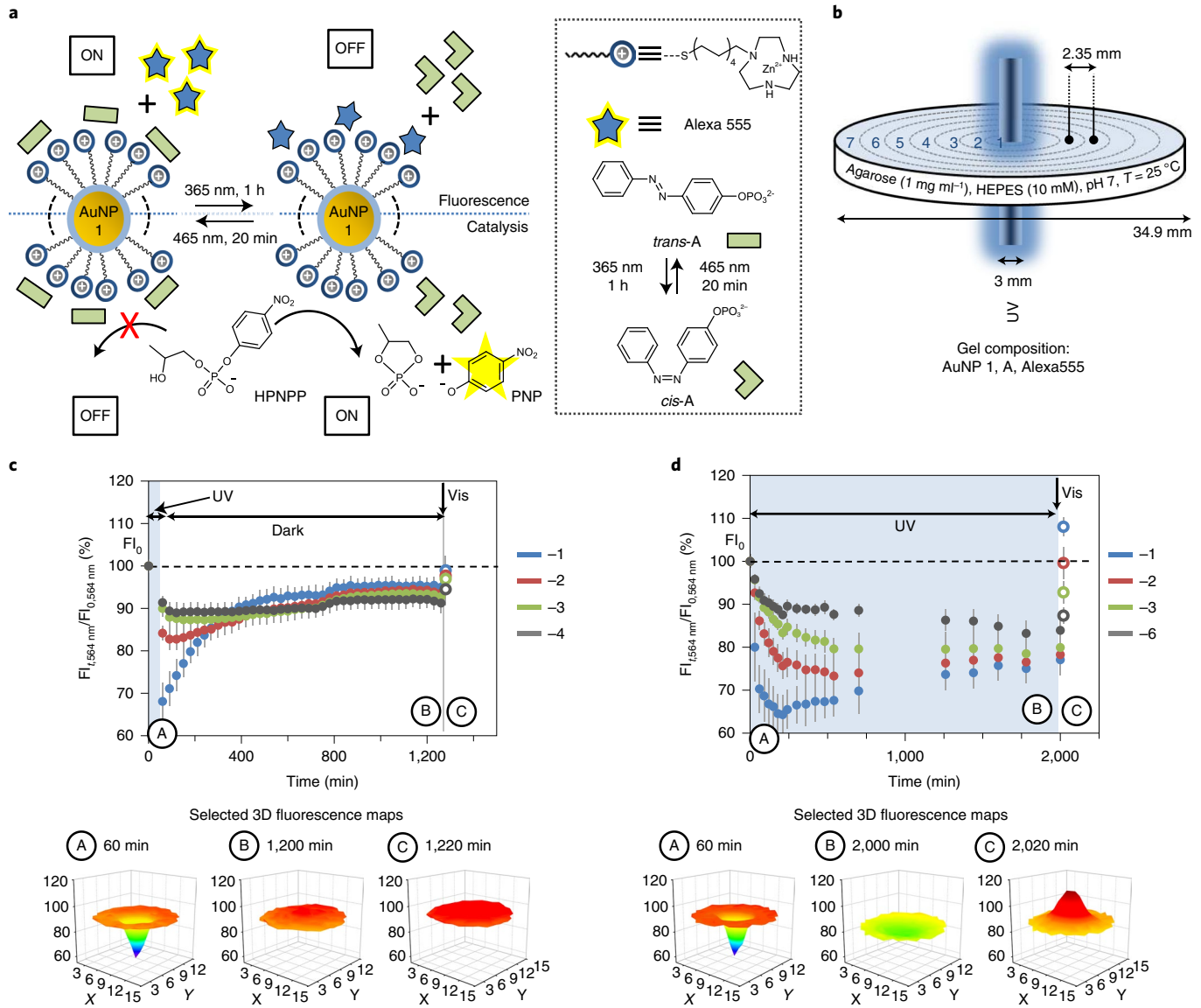

Fig. 1 | Spatially controlled signal generation in a hydrogel. a, Schematic representation that shows how the light-triggered interconversion between *cis*- and *trans*-**A** affects the binding of the fluorophore Alexa555 (fluorescence) and the substrate HPNPP (catalysis) to AuNP **1**. **b**, Experimental setup for local UV irradiation. The numbers indicated in the gel refer to the positions at which either fluorescence or absorbance values were measured. **c**, Changes in the relative fluorescence intensity at 564 nm as a function of time after initial local irradiation of a gel with UV light (365 nm, 60 min) followed by 20 h in the dark and final exposure of the entire gel to vis light (465 nm) for 20 min. The relative intensities are reported for positions 1 (blue), 2 (red), 3 (green) and 6 (dark grey) of the gel. 3D maps of the fluorescence intensities of the entire gel are provided for $t = 60$, 1,200 and 1,220 min as indicated by the encircled letters A–C. Each point is the average of two experiments. Error bars indicate the standard deviation. **d**, Changes in the relative fluorescence intensity at 564 nm as a function of time during continuous local irradiation of a gel with UV light (365 nm, 60 min) for 33 h followed by exposure of the entire gel to vis light (465 nm for 20 min). The relative intensities are reported for positions 1 (blue), 2 (red), 3 (green) and 6 (dark grey) of the gel. 3D maps of the fluorescence intensities of the entire gel are provided for $t = 60$, 2,000 and 2,020 min as indicated by the encircled letters A–C. Each point is the average of three experiments. Error bars indicate the standard deviation.

studies had shown that phosphates have a substantially higher affinity for AuNP **1** compared to carboxylates[19]. Fluorescent probe Alexa555 ($\lambda_{ex/em} = 551/564$ nm) was used in these studies rather than the 6,8-dihydroxy-1,3-pyrenedisulfonic acid probe. Alexa555 has no absorption bands at the wavelengths used for isomerization of **A** (*trans* → *cis*: 365 nm and *cis* → *trans*: 465 nm), which reduces the problem of photobleaching. The improved properties in terms of difference in binding affinity between *cis*- and *trans*-**A** for AuNP **1** and the absence of photobleaching were confirmed by solution studies (Supplementary Fig. 16a).

Our exploration of the systems' properties in a hydrogel started with a study of agarose gel (1 mg ml^{-1}, buffered at pH 7.0) containing AuNP **1** ([TACN·Zn^{2+}] = 20 μM), Alexa555 (0.91 μM) and **A** (10 μM) (Fig. 1b). Gels were prepared in six-well microtiter plates to permit spatially controlled measurement of the fluorescence intensity using multispot analysis. We were pleased to observe that the fluorescence intensity could be reversibly cycled between two values by irradiating the gels sequentially with 365 nm (60 min) and 465 nm (20 min) (Supplementary Fig. 16b,c). A total of five cycles were performed without any notable decrease in signal intensity.

The analogy with the results obtained in solution indicate that the basic working principle of the system, light-induced probe displacement, is not altered in the gel state.

It has been previously demonstrated that spatially controlled irradiation of a solution containing a photoacid, which is a compound that becomes more acidic when irradiated with UV light, locally altered the pH of the solution[20]. Continuous light irradiation resulted in a stationary non-equilibrium situation with a persistent proton gradient, which was exploited to spatially control the rate of a pH-sensitive reaction[21]. Although this approach is an attractive way to maintain a system in a non-equilibrium steady state, a widespread application has been hampered by the high rates of mass transport in solution and the challenge to couple the proton gradient effectively to other chemical processes. We reasoned that both issues could be resolved in our system. First, mass transport in a hydrogel is much slower because it is controlled by diffusion rather than convection. Second, an energy-driven concentration gradient of the photoresponsive element **A** can be coupled to other components through AuNP **1**, which plays a role as transducer element by interacting both with **A** and other species present in the system.

To demonstrate spatially controlled activation by light, the gel was irradiated at 365 nm through a mask containing a 3 mm hole in the centre (Fig. 1b). This indicates that only locally *trans*→*cis*-isomerization of **A** takes place and that only at the corresponding position the relative affinity of Alexa555 for AuNP **1** compared to **A** increases (Supplementary Fig. 17). The fluorescence intensity was measured at positions 1–7, corresponding to areas at increasing distances from the centre.

To understand how local irradiation affected the properties of the system, we carried out two experiments. In a first experiment, the gel was locally irradiated at 365 nm for just 1 h to induce *trans*→*cis*-isomerization and then left in the dark for 20 h (Fig. 1c). It was observed that UV irradiation caused a decrease of fluorescence intensity in position 1 and, to a smaller extent, position 2, but hardly affected the other positions. After having put the gel in the dark, the fluorescent intensities in positions 1 and 2 returned to the original values in around 6 h after which they remained constant. After 20 h in the dark, the entire gel was irradiated at 465 nm for 20 min to ensure complete conversion of *cis*-**A** to *trans*-**A**, but this just caused a very minor increase in the fluorescence intensity (Fig. 1c). On the basis of this final observation it could be concluded that after 20 h in the dark the gel had returned to the original composition before visible light (vis)-irradiation.

Very different observations were made in the second experiment, in which the gel was exposed to continuous local UV irradiation for a period of 33 h (Fig. 1d). Also in this case, the fluorescence intensity in position 1 decreased initially before gradually increasing again. Yet, the increase occurred at a lower rate and the original intensity was never reached. At difference with the previous experiment, the fluorescence intensities in all other positions 2–6 also decreased gradually with a delay time that depended on the distance from position 1. After around 20 h a stable situation was reached with a nearly homogeneous fluorescence intensity all over the gel, which was, however, significantly lower than the original one ($FI_t/FI_0 \approx 0.8$) (three-dimensional (3D) map 2 in Fig. 1d). Exposure of the entire gel to 20 min 465 nm irradiation after this period resulted in a strong peak in fluorescence centred at position 1 with an intensity that was higher than the original one (3D map 3 in Fig. 1d). This observation indicated that continuous local UV irradiation had led to an accumulation of Alexa555 in the centre of the gel.

Kinetic model for the simulation of signal generation under non-equilibrium conditions

To explain these observations a kinetic model was developed that takes into consideration the key kinetic processes that regulate compound distribution in the gel: photoinduced *trans*→*cis*-isomerization of **A**, spontaneous thermally induced back isomerization of **A**, diffusion, and exchange processes occurring on the surface of AuNP **1** (Fig. 2a and Supplementary Fig. 34). The model represents the gel divided in three sectors. Each sector contains all species present in the gel and diffusion is introduced as the kinetic exchange of species of the same kind between sectors. The kinetic parameters of each sector can be individually adjusted; for example, local UV irradiation can be simulated by imposing a high rate constant for *trans*→*cis*-isomerization just in sector 1. Values for the kinetic parameters (related to diffusion, isomerization and dissociation rates) were determined from experimental measurements (see sections 2, 3 and 8 of the Supplementary Information). It is important to note that diffusion-ordered spectroscopy experiments revealed for none of the species a difference in diffusion coefficient between the hydrogel and solution state (Supplementary Table 15). This illustrated that the functional role of the gel matrix is to suppress convection. Moreover, a fivefold lower diffusion coefficient was measured for AuNP **1** compared to the other components, which indicates that on the experimental time scale the diffusion of AuNP **1**, and molecules complexed on its surface (Supplementary Fig. 31), can be ignored.

The kinetic model was used to simulate the two experiments described here. For both cases a plot of the calculated signal intensity in each sector—which is proportional to the concentration of free Alexa555—as a function of time provided profiles that closely matched the experimentally determined ones (compare Fig. 2b to Fig. 1c). The observation that signal evolution in the simulation also matched the experimental time confirmed the validity of the imposed rate constants.

Analysis of the calculated concentrations of each species as a function of time explains how the compound distribution in the gel is affected by local irradiation. The key component that drives the entire process is the photoresponsive element **A**. Spatially controlled irradiation locally converts *trans*-**A** in *cis*-**A** and the lower affinity of the latter for AuNP **1** leads to an increase in the amount of Alexa555 bound to AuNP **1** and hence fluorescence quenching. The local alteration of concentrations in sector 1 installs concentration gradients and the diffusion of species along those gradients. The directional movement of the species emerges from an analysis of the currents, defined as the forward reaction flux minus the backward reaction flux, between the different sectors (Fig. 2c,e). Local irradiation depletes *trans*-**A** in sector 1 that installs a positive current for *trans*-**A** from the other sectors. Oppositely, the local increase in concentration of *cis*-**A** installs negative currents. Capture of Alexa555 on AuNP **1** causes a local depletion of free Alexa555 in sector 1 that also installs a positive current for this species leading to accumulation of the dye in sector 1. For experiment 1, these effects are transient and as soon as irradiation is turned off, the system relaxes slowly back to the equilibrium state (Fig. 2c). At difference, the simulation of experiment 2 illustrates that continuous energy delivery leads to the instalment of a non-equilibrium steady state characterized by persistent currents for *trans*- and *cis*-**A** (Fig. 2e).

An important role in the system is played by AuNP **1**, which acts a transducer element between the photosensitive regulator **A** and Alexa555. Indeed, despite the fact that Alexa555 is not photoresponsive, its local concentration is anyway affected by light irradiation, because Alexa555 is in competition with **A** for binding to AuNP **1**. As long as UV irradiation maintains the high concentration of *cis*-**A** in sector 1, the amount of Alexa555 bound to AuNP **1** will be higher there than in other parts of the gel. In other words, the concentration gradients of *cis*- and *trans*-**A** in the gel are transposed on the surface composition of AuNP **1**. The persistence of a gradient in the surface composition of AuNP **1** in the gel was experimentally observed in the gradient in fluorescent intensity with a maximum at position 1 after exposure of the gel to vis irradiation (Figs. 1d and 2d). It is relevant to emphasize that at the non-equilibrium steady

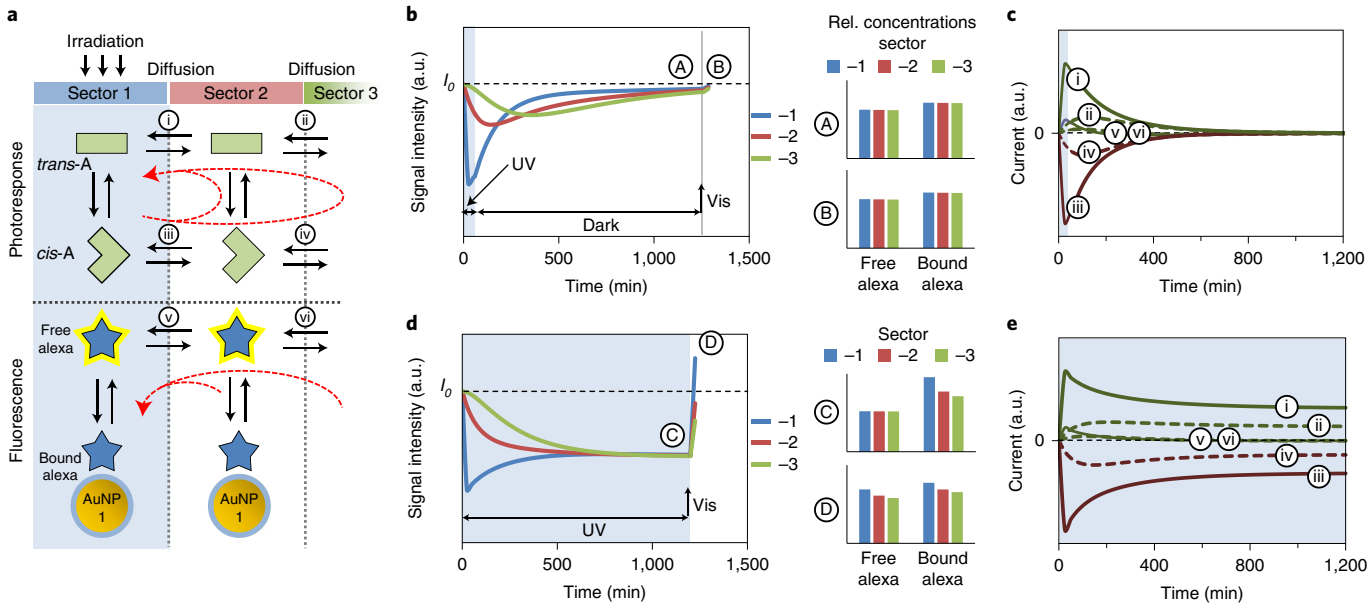

Fig. 2 | Simulations of light-induced diffusion in the hydrogel. a, Kinetic model describing the concentration gradients of the *cis*- and *trans*-isomers of photoresponsive element **A** and the free and bound Alexa555 fluorophore. The model is composed of three sectors 1–3 that communicate through diffusive processes (i)–(vi). A full description of the model can be found in the Supplementary Information (section 9). **b**, Simulated signal intensity as a function of time for the experiment described in Fig. 1c and the relative concentrations of free and bound Alexa555 at times A and B. **c**, Calculated currents in the system (green, positive and brown, negative) as a function of time for the equilibria given in **a** after initial local irradiation followed by a long period in the dark. Solid lines refer to diffusion between sectors 1 and 2, dashed lines refer to diffusion between sectors 2 and 3. **d**, Simulated signal intensity as a function of time for the experiment described in Fig. 1d and the relative concentrations of free and bound Alexa555 at times C and D. **e**, Calculated currents in the system (green: positive, brown: negative) as a function of time for the equilibria given in **a** during continuous local irradiation with UV light. Solid lines refer to diffusion between sectors 1 and 2, dashed lines refer to diffusion between sectors 2 and 3.

state (position C in Fig. 2d) no concentration gradient is present for unbound Alexa555, which is evidenced by the absence of currents for equilibria v and vi (Fig. 2e). This explains the homogeneous fluorescence intensity at the dynamic steady state.

Local catalyst activation through spatially controlled UV irradiation

The observation that the concentration gradient of *cis*- and *trans*-**A** is transposed on the surface composition of AuNP **1**, prompted us to study the catalytic activity of AuNP **1** in the transphosphorylation of HPNPP under non-equilibrium steady-state conditions (Fig. 1a). A characteristic feature of enzyme catalysis is that the reaction rates are described by Michaelis–Menten saturation kinetics, which indicates that complex formation between substrate and enzyme precedes the catalytic event[22]. Consequently, the extend of enzyme saturation by the substrate plays an important role in determining the reaction rate (see next). Considering that also the catalytic activity of AuNP **1** in the transphosphorylation of HPNPP can be described using similar saturation kinetics[14], we were intrigued to find out whether the instalment of a gradient in AuNP **1** surface composition under non-equilibrium conditions would result in spatially differentiated catalytic activity. Agarose gels (1 mg ml^{-1}, buffered at pH 7.0) were prepared containing AuNP **1** ([TACN·Zn^{2+}] = 40 μM), *trans*-**A** (30 μM) and HPNPP (1 mM). Concentrations were optimized to have the maximum difference in rate between the *cis*- and *trans*-isomers of **A**. Reactions could be conveniently monitored by measuring the absorbance at 413 nm—which corresponds to the isosbestic point of *cis*- and *trans*-**A**—originating from the liberated *p*-nitrophenol product.

The first experiment aimed at demonstrating that the presence of either *trans*- or *cis*-**A** in the gel affected the catalytic activity of AuNP **1** to different extents. For *trans*-**A**, this indicated keeping the gel in the dark and measuring the absorbance at regular time intervals. To study the effect of *cis*-**A** on the catalytic activity the entire gel was kept under continuous UV irradiation with short interruptions to measure the absorbance. The absorbance was measured at different areas of each gel corresponding to the positions 1–7. It was found that in both cases, the average absorbance increased homogeneously all over the gels (Fig. 3b, open circles). The measurements confirmed the higher catalytic activity of AuNP **1** in the presence of *cis*-**A**, which is consistent with the lower affinity of *cis*-**A** for AuNP **1**. Exposure of both gels to vis irradiation after 12 h caused a notable change in rate for the gel containing *cis*-**A**, caused by the conversion of *cis*-**A** in the stronger inhibitor *trans*-**A**. For the gel containing *trans*-**A** no change in rate was observed after vis irradiation (Fig. 3b, open circles).

Catalytic activity was then studied under non-equilibrium conditions installed by continuous local UV irradiation of the centre of a gel prepared with *trans*-**A**. Control experiments showed that local UV irradiation did not install temperature gradients in the gel (Supplementary Fig. 21c). Absorbance data was again spatially collected for positions 1–7. At difference with the all-*cis* or all-*trans* gels, the increase in rate was not homogeneous (Fig. 3b, filled circles). The rate was highest in position 1 and gradually decreased as the distance from the irradiation centre increased. Yet, the rate in position 1 was substantially lower than the rate observed for the gel containing just *cis*-**A** and the differences in rate between positions 1–6 were relatively modest. Exposure of the entire gel to vis irradiation after 12 h caused a transient delay in the increase in absorbance in positions close to the centre, after which the absorbance continued to increase homogeneously all over the gel (Fig. 3b, filled circles). Overall, the data show a spatially differentiated catalytic response to local irradiation. In addition, the fact that 20 min vis irradiation after 12 h induced a local change indicated that the

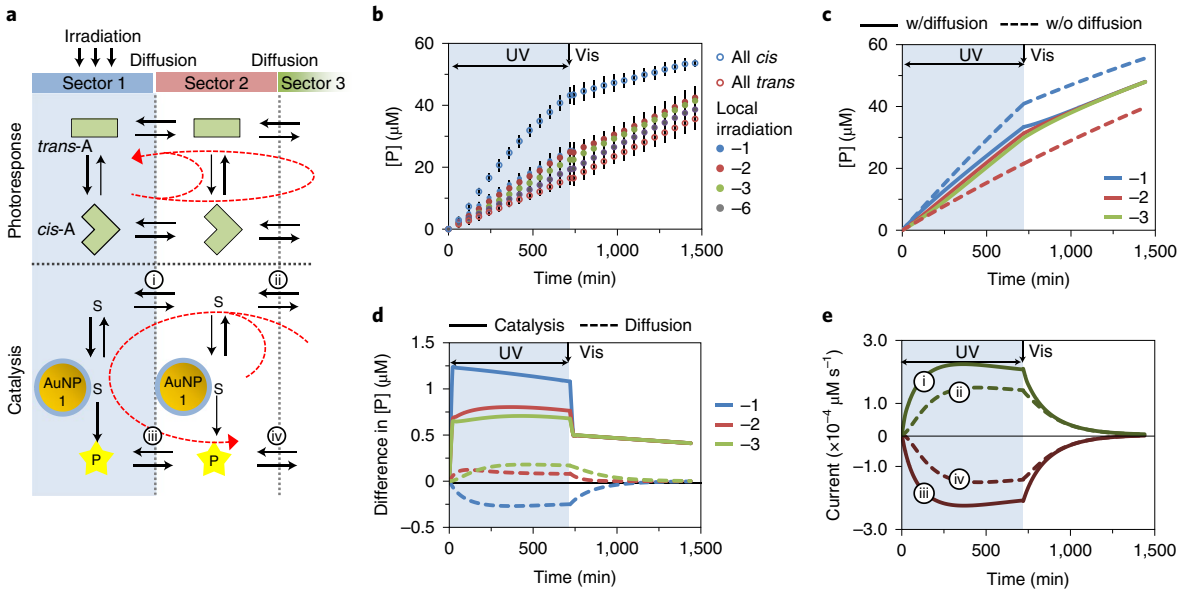

Fig. 3 | Experimental and simulated catalytic activity on local irradiation. a, Kinetic model describing the concentration gradients of the *cis*- and *trans*-isomers of photoresponsive element **A**, substrate and product. A full description of the model can be found in the Supplementary Information (section 10). **b**, Increase in concentration of product (*p*-nitrophenol) as function of time in an agarose gel (1 mg ml^{-1}) containing AuNP **1** ([TACN·Zn^{2+}] = 40 μM), *trans*-**A** (30 μM) and HPNPP (1 mM). Gels were kept in the dark (all *trans*, open red circles), exposed entirely to UV irradiation (all *cis*, open blue circles) or irradiated with UV irradiation just in the centre through a mask (coloured filled circles 1–3, 6). For the first two cases, the concentrations were taken as average values of positions 1–6. In the third case, the concentrations were measured at different distances from the centre (positions 1–3 and 6 in Fig. 1b). After 12 h all gels were exposed to vis irradiation for 20 min after which the measurements were continued. Each point is the average of three experiments. Error bars indicate the standard deviation. **c**, Product concentrations in each sector as a function of time simulated using the model in the absence (dashed lines) and presence (solid lines) of diffusion between the sectors. **d**, Calculated changes in the product concentration in each sector originating from catalysis (solid lines) and diffusion (dashed lines). **e**, Calculated currents (green, positive and brown, negative) in the system as a function of time for the equilibria (i)–(iv) depicted in **a**. Solid lines refer to diffusion between sectors 1 and 2, dashed lines refer to diffusion between sectors 2 and 3.

system was indeed in a stationary non-equilibrium state. However, the absolute differences in rate between the different positions in the gel appeared relatively modest, particularly when compared to the differences observed for the homogeneous gels containing just *cis*- or *trans*-**A**. Therefore, we developed a theoretical kinetic framework to explain these results.

Kinetic model to describe local catalysis enhancement under non-equilibrium conditions

A catalytic process was introduced to the previous model (Fig. 3a and Supplementary Fig. 35) that involved complex formation between HPNPP and AuNP **1** followed by conversion of HPNPP in product. A lower affinity of HPNPP for AuNP **1** compared to both *cis*- and *trans*-**A** was imposed, in correspondence with the experimental observation that low μM concentrations of **A** are sufficient to inhibit catalysis when HPNPP is present at a concentration of 1 mM. The rate constant for product formation was set to 3×10^{-3} s^{-1}, which is in line with the experimentally determined k_{cat} value reported earlier for AuNP **1** (ref. [23]). All other rate constants were left unvaried compared to the model used to simulate signal evolution. Concentrations were imposed such that the model also provided a quantitative response in line with the experimental values.

In the first simulation, a high rate constant for *trans* → *cis*-isomerization of **A** was imposed only in sector 1 to simulate local irradiation with UV light, but without allowing diffusion between sectors. The scope of this simulation was to compare the intrinsic rates of product formation in the presence of either *cis*-**A** (in sector 1) or *trans*-**A** (in sectors 2 and 3). The simulated relative rates compared well to the experimental data obtained for the homogeneous gels containing either *trans*- or *cis*-**A** indicating that the kinetic parameters were properly set (compare Fig. 3c, dashed lines to Fig. 3a, open circles). The simulation of an exposure of this gel to vis irradiation after 12 h caused a reduction in the rate in sector 1, but did not change the rates in sectors 2 and 3 that already contained *trans*-**A**. This result too was in agreement with the experimental data.

Next, the simulation was repeated permitting diffusion of the species between sectors 1–3. This simulation accurately reproduced the key experimental observations under continuous irradiation: in all sectors the product increase occurred with an intermediate rate between the ones observed in the presence of *cis*- or *trans*-**A** and the rate in sector 1 was slightly higher than those in sectors 2 and 3 (Fig. 3c, solid lines). A simulation of the exposure to vis irradiation after 20 h neatly reproduced the experimentally observed temporary decrease in rate in sector 1 before the rates in all sectors became equal (compare Fig. 3c, solid lines to Fig. 3a, filled circles).

Given that the model described the experiments with good accuracy, we analysed what happened inside the gel on continuous local irradiation. The model provided the concentrations of all species as a function of time, which permitted for each sector a calculation of the fraction of product that originated from catalysis and from diffusion (Fig. 3d). These calculations confirmed the higher catalytic activity in sector 1 compared to sectors 2 and 3 originating from a higher concentration of the weak inhibitor *cis*-**A** in that sector and, consequently, a higher surface saturation of AuNP **1** with HPNPP. Yet, the increased catalytic production in sector 1 is counterbalanced by a decrease in product concentration caused by diffusion to sectors 2 and 3. On the contrary, the lower catalytic activities in sectors 2 and 3 are compensated by a positive influx of product originating from sector 1. The net result is that the concentration of

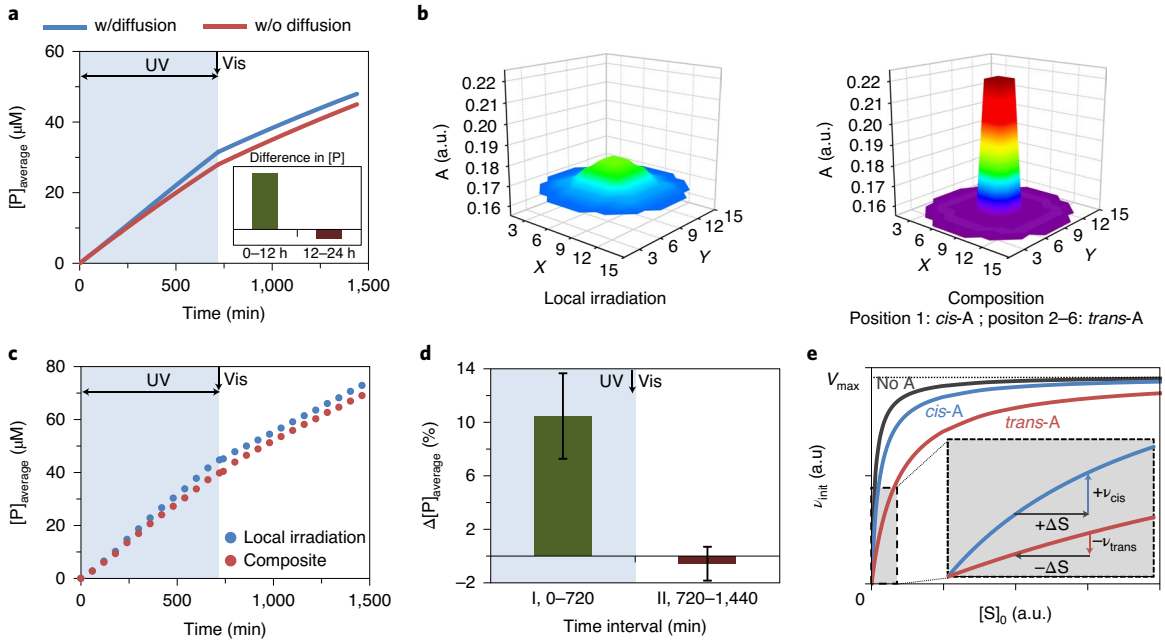

Fig. 4 | Enhanced catalysis under non-equilibrium conditions. a, Simulated increase in the average product concentration in sectors 1–3 using the kinetic model depicted in Fig. 3a with (blue line) and without (red line) diffusion. The inset demonstrates the difference in product increase between the two cases for the first (0–12 h) and second (12–24 h) period. **b**, 3D plot of the measured absorbance values in a gel after local irradiation for 12 h (left) and 3D plot of a composition of the absorbance in position 1 of an all-*cis* gel and positions 2–6 of an all-*trans* gel (right), the values are the average of two experiments. Agarose gel (1 mg ml^{-1}) contained AuNP **1** ([TACN·Zn^{2+}] = 40 μM), *trans*-**A** (30 μM) and HPNPP (1.5 mM). Gels were kept in the dark (all *trans*), exposed entirely to UV irradiation (all *cis*) or irradiated with UV irradiation just in the centre through a mask. After 12 h, all gels were exposed to vis irradiation for 20 min after which the measurements were continued. The absorbance was measured at different areas of each gel corresponding to the positions 1–7. **c**, Product concentration averaged over position 1–6 as a function of time for a gel that was locally irradiated (blue) and the product concentration averaged over position 1 of an all-*cis* gel and positions 2–6 of an all-*trans* gel (red). **d**, Difference in product increase between the cases described in Fig. 4c for the first (I, 0–12 h) and second (II, 12–24 h) period. The values are the average of three sets of measurements and the error bars give the standard deviation. **e**, Calculated Michaelis–Menten saturation profiles for the AuNP **1**-mediated conversion of HPNPP in the absence of inhibitor (grey curve), in the presence of *cis*-**A** (blue curve) and *trans*-**A** (red curve). The inset shows how in the second-order kinetic regime the decrease in rate caused by a decreased concentration of substrate in the presence of *trans*-**A** (red curve) is lower than the increase in rate induced by a higher concentration of substrate in the presence of *cis*-**A** (blue curve).

product increases more or less homogeneously in all sectors despite the substantial differences in catalytic activity between sector 1 and sectors 2 and 3.

An analysis of the currents in the system revealed a marked difference with the diffusion experiments involving Alexa555 (Fig. 3e). For the fluorescence study, it was observed that at the stationary non-equilibrium state no gradient was present for unbound Alexa555 (currents 5 and 6 in Fig. 2e). In contrast, in the catalysis experiment concentration gradients are maintained also for unbound substrate and product under non-equilibrium conditions. The reason for this difference is that the initial offset in substrate concentration on local irradiation is maintained because of the continuous catalytic conversion of substrate in product. The enhanced depletion of substrate in sector 1 compared to the sectors 2 and 3 causes sustained diffusion of the substrate to the area of highest catalytic activity. Oppositely, the enhanced formation of product in that area leads to a sustained diffusion away from the reaction centre. Experimental evidence in confirmation of this analysis can be found in the temporary decrease in the rate of product accumulation in sector 1 after exposure to vis irradiation (Fig. 3b). Whereas vis irradiation rapidly reduces the catalytic activity in sector 1 to the same level as sectors 2 and 3, it takes a longer time before the gradient in product concentration disappeared because of the low diffusion rates (Fig. 3d). The net result is that for a limited amount of time, the concentration of product in sector 1 increases slower than in sectors 2 and 3. Eventually a stationary state is reached in which concentration gradients in the gel are absent and the product concentration increases homogeneously throughout the gel.

Diffusion leads to an enhanced overall catalytic activity

The simulations carried out with and without diffusion between sectors represent different situations that can be interpreted as an open and closed system, respectively, to which the same amount of energy is provided. Comparison between the two simulations therefore provided a means to analyse to which extent diffusional processes affect the efficiency at which the provided energy is exploited. Comparison of the overall catalytic activity in each system, calculated by taking the average of the rates of sectors 1–3, revealed a notably higher catalytic activity in the open system amounting to an increased product concentration of around 12% after 720 min. Stimulated by this sizeable difference, we sought to measure it experimentally. The challenge lied in finding an experimental analogue for a closed system to be compared with the open system described in the previous section. We reasoned that the activity of a closed system could be approximated by averaging the rate of position 1 from the all-*cis* gel and the rates of positions 2–6 from the all-*trans* gel, yielding a composite system very similar to the one simulated as the closed system (Fig. 4b). Measurements were performed three times and the data was analysed as described in Supplementary Fig. 36. Comparison of the average rate between the 'open' and 'closed' system confirmed the increased activity in the open system with an increase of 10.5 ± 3.2% compared to the closed

system during continuous irradiation (Fig. 4d). The fact that the difference in activity disappeared after vis irradiation validated the method and confirmed that the increased activity originated from the conditions installed under continuous UV irradiation (Fig. 4d).

Analysis of the species distribution as calculated by the model showed that the higher activity of the open system can be attributed to two concentration gradients. The first and greater effect originates from the higher overall concentration of the weaker inhibitor *cis*-**A** in the open system. Diffusion of this high-energy species to the non-irradiated parts of the gel affects the catalytic rates in those areas until *cis*-**A** dissipates energy by returning to *trans*-**A** and diffusing back to the centre. The second effect originates from substrate diffusion to the centre where it is converted at a higher rate compared to the other parts of the gel due to the higher local concentration of *cis*-**A** in the centre (see inset Fig. 4e). The decrease in rate ($-\nu_{trans}$) caused by the diffusion of substrate away from an area with high concentration of *trans*-**A** is smaller than the increase in rate ($+\nu_{cis}$) caused by the same amount of substrate in an area enriched in *cis*-**A**. The result is a net gain in overall catalytic activity in the system sustained by a substrate gradient.

The increased activity in the open system depends in a non-linear manner on the substrate concentrations owing to the Michaelis–Menten-like catalytic behaviour of the nanoparticles. Additional simulations at different substrate concentrations showed that the difference between closed and open systems may increase up to 21% by reducing the substrate concentration (Supplementary Fig. 37). The reason is that at lower substrate concentrations, at which the catalyst is not saturated, the difference in reaction rate caused by *cis*- or *trans*-**A** is larger as can be observed from the calculated saturation profiles in the presence of either inhibitor (Fig. 4e). The result is that concentration gradients under non-equilibrium conditions exert a larger effect on the overall activity of the system.

Conclusions

In conclusion, we have shown that continuous local irradiation of a hydrogel results in the sustained directional diffusion of a photoresponsive element in the gel. The directional movement can be interpreted as a macroscopic expression of kinetic asymmetry in the energy consumption pathway that drives molecular systems away from equilibrium[24–27]. On the macroscopic level discussed here, the thermodynamic equilibrium refers to concentrations at different locations of the gel. Spatially controlled energy delivery installs asymmetry in the matrix leading to concentration gradients of the chemical species involved. The resulting concentration gradients of the photoresponsive element are transposed on the concentrations of other small molecules through competitive binding to a gold nanoparticle with much lower diffusion rate. The different saturation levels of the nanoparticle surface affect the fluorescent and catalytic properties of the system. It is shown that diffusional processes contribute to an enhanced overall catalytic productivity of the system under non-equilibrium conditions. Our simulations indicate that the superimposition of a linear concentration gradient and a non-linear systems response (for example, enzyme-like catalysis or cooperative self-assembly) is a particularly attractive target for further research in macroscopic out-of-equilibrium studies.

Online content

Any methods, additional references, Nature Research reporting summaries, source data, extended data, supplementary information, acknowledgements, peer review information; details of author contributions and competing interests; and statements of data and code availability are available at https://doi.org/10.1038/s41565-020-0734-1.

Received: 21 January 2020; Accepted: 12 June 2020;
Published online: 20 July 2020

References

1. Branscomb, E., Biancalani, T., Goldenfeld, N. & Russell, M. Escapement mechanisms and the conversion of disequilibria; the engines of creation. *Phys. Rep.* **677**, 1–60 (2017).
2. Gnesotto, F. S., Mura, F., Gladrow, J. & Broedersz, C. P. Broken detailed balance and non-equilibrium dynamics in living systems: a review. *Rep. Prog. Phys.* **81**, 066601 (2018).
3. Astumian, R. D. Microscopic reversibility as the organizing principle of molecular machines. *Nat. Nanotechnol.* **7**, 684–688 (2012).
4. Desai, A. & Mitchison, T. J. Microtubule polymerization dynamics. *Annu. Rev. Cell Dev. Biol.* **13**, 83–117 (1997).
5. Feher, J. *Quantitative Human Physiology* (Academic Press, 2017).
6. Kicheva, A., Cohen, M. & Briscoe, J. Developmental pattern formation: insights from physics and biology. *Science* **338**, 210–212 (2012).
7. Wang, W., Duan, W. T., Ahmed, S., Mallouk, T. E. & Sen, A. Small power: autonomous nano- and micromotors propelled by self-generated gradients. *Nano Today* **8**, 531–554 (2013).
8. Mattia, E. & Otto, S. Supramolecular systems chemistry. *Nat. Nanotechnol.* **10**, 111–119 (2015).
9. Grzybowski, B. A. & Huck, W. T. S. The nanotechnology of life-inspired systems. *Nat. Nanotechnol.* **11**, 584–591 (2016).
10. Ashkenasy, G., Hermans, T. M., Otto, S. & Taylor, A. F. Systems chemistry. *Chem. Soc. Rev.* **46**, 2543–2554 (2017).
11. Astumian, R. D. Design principles for brownian molecular machines: how to swim in molasses and walk in a hurricane. *Phys. Chem. Chem. Phys.* **9**, 5067–5083 (2007).
12. Kassem, S. et al. Artificial molecular motors. *Chem. Soc. Rev.* **46**, 2592–2621 (2017).
13. Prins, L. J. Emergence of complex chemistry on an organic monolayer. *Acc. Chem. Res.* **48**, 1920–1928 (2015).
14. Manea, F., Houillon, F. B., Pasquato, L. & Scrimin, P. Nanozymes: gold-nanoparticle-based transphosphorylation catalysts. *Angew. Chem. Int. Ed.* **43**, 6165–6169 (2004).
15. Pieters, G., Cazzolaro, A., Bonomi, R. & Prins, L. J. Self-assembly and selective exchange of oligoanions on the surface of monolayer protected Au nanoparticles in water. *Chem. Commun.* **48**, 1916–1918 (2012).
16. Sapsford, K. E., Berti, L. & Medintz, I. L. Materials for fluorescence resonance energy transfer analysis: beyond traditional donor-acceptor combinations. *Angew. Chem. Int. Ed.* **45**, 4562–4588 (2006).
17. Neri, S., Martin, S. G., Pezzato, C. & Prins, L. J. Photoswitchable catalysis by a nanozyme mediated by a light-sensitive cofactor. *J. Am. Chem. Soc.* **139**, 1794–1797 (2017).
18. Wei, H. & Wang, E. K. Nanomaterials with enzyme-like characteristics (nanozymes): next-generation artificial enzymes. *Chem. Soc. Rev.* **42**, 6060–6093 (2013).
19. Pezzato, C., Scrimin, P. & Prins, L. J. Zn^{2+}-regulated self-sorting and mixing of phosphates and carboxylates on the surface of functionalized gold nanoparticles. *Angew. Chem. Int. Ed.* **53**, 2104–2109 (2014).
20. Le Saux, T., Plasson, R. & Jullien, L. Energy propagation throughout chemical networks. *Chem. Commun.* **50**, 6189–6195 (2014).
21. Emond, M. et al. Energy propagation through a protometabolism leading to the local emergence of singular stationary concentration profiles. *Chem. Eur. J.* **18**, 14375–14383 (2012).
22. Fersht, A. *Structure and Mechanism in Protein Science. A Guide to Enzyme Catalysis and Protein Folding* (W. H. Freeman and Company, 1999).
23. Pezzato, C. & Prins, L. J. Transient signal generation in a self-assembled nanosystem fueled by ATP. *Nat. Commun.* **6**, 7790 (2015).
24. Astumian, R. D. Stochastic pumping of non-equilibrium steady-states: how molecules adapt to a fluctuating environment. *Chem. Commun.* **54**, 427–444 (2018).
25. Ragazzon, G. & Prins, L. J. Energy consumption in chemical fuel-driven self-assembly. *Nat. Nanotechnol.* **13**, 882–889 (2018).
26. Astumian, R. D. Kinetic asymmetry allows macromolecular catalysts to drive an information ratchet. *Nat. Commun.* **10**, 3837 (2019).
27. Penocchio, E., Rao, R. & Esposito, M. Thermodynamic efficiency in dissipative chemistry. *Nat. Commun.* **10**, 3865 (2019).

Data availability

The data that support the findings of this study are available from the corresponding author on reasonable request.

Acknowledgements

The research was financially supported by the China Science Council (R.C.) and the Italian Ministry of Education and Research (L.J.P., grant no. 2017E44A9P). T. Carofiglio is acknowledged for preparation of the masks. J. Czescik is acknowledged for providing the substrate HPNPP. M. Troiani is acknowledged for contributing to the synthesis of compound **A**.

Author contributions

R.C. and L.J.P. designed the experiments. R.C. carried out all experiments. S.N. performed preliminary experiments. L.J.P. wrote the kinetic models and performed the simulations. R.C. and L.J.P. wrote the manuscript.

Competing interests

The authors declare no competing interests.

Additional information

Supplementary information is available for this paper at https://doi.org/10.1038/s41565-020-0734-1.

Correspondence and requests for materials should be addressed to L.J.P.

Reprints and permissions information is available at www.nature.com/reprints.